

ARMY RESEARCH LABORATORY



**Mechanical Response of an Al-PTFE Composite to Uniaxial
Compression Over a Range of Strain Rates and
Temperatures**

by Daniel T. Casem

ARL-TR-4560

September 2008

NOTICES

Disclaimers

The findings in this report are not to be construed as an official Department of the Army position unless so designated by other authorized documents.

Citation of manufacturer's or trade names does not constitute an official endorsement or approval of the use thereof.

Destroy this report when it is no longer needed. Do not return it to the originator.

Army Research Laboratory

Aberdeen Proving Ground, MD 21005-5069

ARL-TR-4560

September 2008

Mechanical Response of an Al-PTFE Composite to Uniaxial Compression Over a Range of Strain Rates and Temperatures

Daniel T. Casem

Weapons and Materials Research Directorate, ARL

REPORT DOCUMENTATION PAGE			Form Approved OMB No. 0704-0188		
Public reporting burden for this collection of information is estimated to average 1 hour per response, including the time for reviewing instructions, searching existing data sources, gathering and maintaining the data needed, and completing and reviewing the collection information. Send comments regarding this burden estimate or any other aspect of this collection of information, including suggestions for reducing the burden, to Department of Defense, Washington Headquarters Services, Directorate for Information Operations and Reports (0704-0188), 1215 Jefferson Davis Highway, Suite 1204, Arlington, VA 22202-4302. Respondents should be aware that notwithstanding any other provision of law, no person shall be subject to any penalty for failing to comply with a collection of information if it does not display a currently valid OMB control number. PLEASE DO NOT RETURN YOUR FORM TO THE ABOVE ADDRESS.					
1. REPORT DATE (DD-MM-YYYY) September 2008		2. REPORT TYPE Final		3. DATES COVERED (From - To) October 2006–April 2008	
4. TITLE AND SUBTITLE Mechanical Response of an Al-PTFE Composite to Uniaxial Compression Over a Range of Strain Rates and Temperatures			5a. CONTRACT NUMBER		
			5b. GRANT NUMBER		
			5c. PROGRAM ELEMENT NUMBER		
6. AUTHOR(S) Daniel T. Casem			5d. PROJECT NUMBER 611102H42		
			5e. TASK NUMBER		
			5f. WORK UNIT NUMBER		
7. PERFORMING ORGANIZATION NAME(S) AND ADDRESS(ES) U.S. Army Research Laboratory ATTN: AMSRD-ARL-WM-TD Aberdeen Proving Ground, MD 21005-5069			8. PERFORMING ORGANIZATION REPORT NUMBER ARL-TR-4560		
9. SPONSORING/MONITORING AGENCY NAME(S) AND ADDRESS(ES)			10. SPONSOR/MONITOR'S ACRONYM(S)		
			11. SPONSOR/MONITOR'S REPORT NUMBER(S)		
12. DISTRIBUTION/AVAILABILITY STATEMENT Approved for public release; distribution is unlimited.					
13. SUPPLEMENTARY NOTES					
14. ABSTRACT Compressive stress-strain curves were generated for a pressed and sintered mixture of polytetrafluoroethylene and aluminum powders. Experiments were performed at strain rates ranging from 0.001 to 8000/s using a servo-hydraulic load frame and a split Hopkinson pressure bar. High-rate experiments were also performed over a temperature range of 22–78 °C. The data is fit to the Johnson-Cook and Modified Johnson-Cook constitutive equations and also to a Zerilli-Armstrong equation adapted for use with polymers. Although the material is known to be reactive, only the inert behavior is described in this report.					
15. SUBJECT TERMS reactive material, split Hopkinson pressure bar, Zerilli-Armstrong polymer model					
16. SECURITY CLASSIFICATION OF:			17. LIMITATION OF ABSTRACT	18. NUMBER OF PAGES	19a. NAME OF RESPONSIBLE PERSON
a. REPORT	b. ABSTRACT	c. THIS PAGE			Daniel T. Casem
UNCLASSIFIED	UNCLASSIFIED	UNCLASSIFIED	UL	28	19b. TELEPHONE NUMBER (Include area code) 410-306-0972

Contents

List of Figures	iv
List of Tables	v
1. Introduction	1
2. Material	1
3. Experimental Procedure	2
3.1 Low-Rate Tests.....	2
3.2 High-Rate Tests.....	2
3.3 Temperature Tests.....	2
4. Results	3
5. Constitutive Modeling	8
5.1 Johnson-Cook and Modified Johnson Cook.....	8
5.2 Zerilli-Armstrong Model for Polymers.....	11
6. Conclusion	12
7. References	15
Appendix. Strain Measures Defined	17
Distribution List	19

List of Figures

Figure 1. Engineering stress vs. engineering strain for Al/PTFE (compression). All specimens were initially at room temperature (22 °C).	3
Figure 2. Lateral strain as measured by a laser extensometer in the SHPB tests plotted in figure 1 (thin black curves). The heavy red curve shows that which would be expected from incompressible behavior.....	4
Figure 3. True stress-strain curves for Al/PTFE. All samples were initially at room temperature (22 °C).	5
Figure 4. The data of figure 3 repeated on a finer scale to illustrate the low-strain behavior.	5
Figure 5. The variation of true strain rate for the SHPB tests.....	6
Figure 6. Strain-rate hardening observed in the experiments compared to the MJC, JC, and ZA fits. Stress is measured at 7% total true strain, all at room temperature (295 K).	6
Figure 7. Stress-strain curves obtained at a rate of 4000/s over a range of initial temperatures.....	7
Figure 8. Three fits to the high-rate temperature data (10% total strain, 4000/s). The JC equation is fit over two temperature ranges: the lower temperature range of $295 \text{ K} \leq T \leq 329 \text{ K}$ and the full temperature range. A fit is also shown for the ZA model (full range).	7
Figure 9. MJC model predictions, assuming adiabatic conditions, compared to the high-rate (SHPB) data. The JC model predictions are essentially identical.	10
Figure 10. MJC model predictions, assuming isothermal deformations, compared to the low-rate experiments. The JC model predictions are essentially identical.	10
Figure 11. Comparison of the ZA model to the SHPB experiments assuming adiabatic conditions.....	13
Figure 12. Comparison of the ZA model to the low-rate experiments assuming isothermal conditions. Note the great improvement over the JC fits to the same data, figure 10.	14

List of Tables

Table 1. JC and MJC constants for Al/PTFE. The fits are performed over two temperature ranges.	9
Table 2. The ZA constants for Al/PTFE. The values determined by Cai et al. (13) and Zerilli and Armstrong (11) for PTFE-Al-W and PTFE are included for comparison.	13

INTENTIONALLY LEFT BLANK.

1. Introduction

Reactive materials can be loosely categorized as composites of inert solid materials which, when subjected to a violent mechanical stimulus such as an impact, react exothermally with a rapid release of energy. This reaction, while aptly described as “explosive,” differs from a true detonation or deflagration in that it requires a mechanical stimulus to not only initiate the reaction but also to sustain it. Such materials can also be fairly robust mechanically and can serve as substantial structural components. Because of these properties, reactive materials have a number of potential ordnance applications. Various compositions have been investigated to tailor properties of reactivity, strength, and density, to suit particular needs.

This report addresses a specific aluminum/polytetrafluoroethylene (Al/PTFE) formulation that serves as an important benchmark for current reactive material development. In addition to material development, a good deal of work is underway to develop physics-based modeling capabilities for reactive materials. To aid in this latter effort, this report provides basic constitutive models for the inert behavior of this material. Compression tests have been performed over a range of strain rates and temperatures relevant to the conditions present during low-speed impact. This data, presented in the following sections, is used to generate parameters for both the Johnson-Cook (JC) and Modified Johnson-Cook (MJC) constitutive models. Although not ideally suited to represent this material, these parameters are given primarily due to the wide-spread use of these models and their availability in the current suite of hydrocodes. An additional, and more appropriate, fit is given for the Zerilli-Armstrong (ZA) model for polymers.

The remainder of this document is organized as follows: a basic material description is given in section 2; section 3 describes the testing techniques used in the experiments, and the data is presented in section 4; finally, the model parameters and descriptions of the fitting processes are given in section 5. Unless otherwise noted, the use of the words “stress” and “strain” denote positive values in compression.

2. Material

The samples tested during this program were supplied by General Sciences, Inc. (GSI). They were made from a material designated by GSI as GSI-0017. It is a pressed and sintered mixture of aluminum and PTFE powders, 26.5% and 73.5% by weight, respectively. The initial powder sizes are 44 and 31 μm , respectively. The density of the compacted material, as measured by a buoyancy method based on Archimedes principle, is 2.29 g/cm^3 . The longitudinal wave speed, measured by ultrasound at 10 MHz, is 1570 m/s.

3. Experimental Procedure

3.1 Low-Rate Tests

Low-rate tests were performed with an Instron, Inc., model 1331 servo-hydraulic load frame. The load applied to the specimen was measured with a load cell, and the specimen deformation was measured using a linear variable differential transformer (LVDT) measurement of the cross-head displacement and includes a correction for machine compliance. The specimens were cylindrical, nominally 6.35 mm in both diameter and length. Contact surfaces were lubricated with a heat-stable silicone lubricant. All of the low-rate tests were performed at room temperature (22 °C).

3.2 High-Rate Tests

A 6.35-mm-diameter 7075-T6 aluminum Split Hopkinson Pressure Bar (SHPB) was used for the high-rate tests. A series of six tests were performed at rates from 600 to 8000/s, all initially at room temperature (22 °C). The specimens were cylindrical, 3.18 mm in diameter and length, and contact surfaces were lubricated with the same silicone lubricant used in the low-rate tests. All data analysis accounts for bar-wave dispersion using a method based on Follansbee and Franz (1) and Gong et al. (2).

As is typical with the SHPB, axial deformation of the specimen is determined by the bar analysis (see, for example, Follansbee [3]). However, the radial deformation is unknown, and is usually determined under the assumption that the deformation (both elastic and inelastic) in the specimen occurs at constant volume. To verify this assumption, a laser extensometer (also known as a laser occlusive radius detector, or LORD [4]) was used to measure the radial deformation of the specimens during dynamic compression. The frequency response of this device is very high (~10 MHz), and in our experience it is able to resolve deformations as small as 0.01 mm. The results of these experiments are discussed in section 4.

3.3 Temperature Tests

A final set of experiments was performed at elevated temperatures to quantify the thermal softening behavior of the material. These were performed at a consistent strain rate of 4000/s using the SHPB. Heating was accomplished by circulating heated air into a chamber which enclosed the specimen and the adjacent ~65 mm sections of the bars. Ideally, specimen temperature would have been monitored directly with a thermocouple glued to each specimen. However, this proved impractical because of the small sample size and also because of the difficulty in adhering gages to the specimen.* Instead, specimen temperature was measured with a thermocouple probe placed within 1 cm of the specimen, i.e., the probe measures ambient air

* PTFE, more commonly known as Teflon, is widely known for its “non-stick” properties.

temperature and not the specimen temperature directly. The temperature in the chamber was allowed to equilibrate over a 20 min period prior to each test to ensure that the specimen and relevant sections of the bars were allowed to reach the ambient temperature. The temperature gradient in the bars is believed to have negligible effects on the bar wave propagation and the strain gage measurements. Temperature measurements made in this way are estimated to be accurate to within ± 2 °C.

4. Results

Figure 1 shows the engineering stress-strain curves obtained from the room temperature tests. Because of the brief duration of the deformation, the high rate curves (600/s and beyond) are considered adiabatic. In contrast, the lowest rate curves, 0.001 and 0.01/s, are considered isothermal. The intermediate rate, at 0.1/s, is probably somewhere between the two limits.

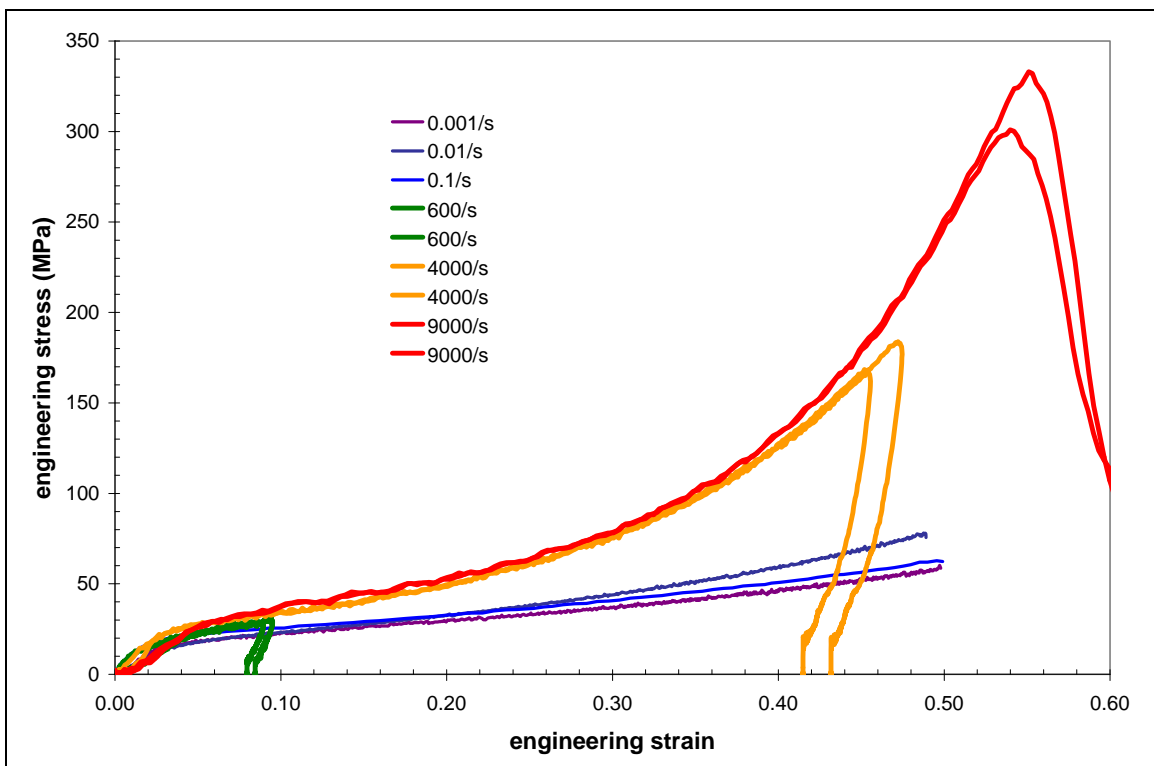


Figure 1. Engineering stress vs. engineering strain for Al/PTFE (compression). All specimens were initially at room temperature (22 °C).

Figure 2 shows the tensile radial engineering strain as measured by the laser extensometer as a function of compressive axial engineering strain for the six SHPB experiments shown in figure 1. These are plotted as thin black curves. The heavy red curve is the relationship that

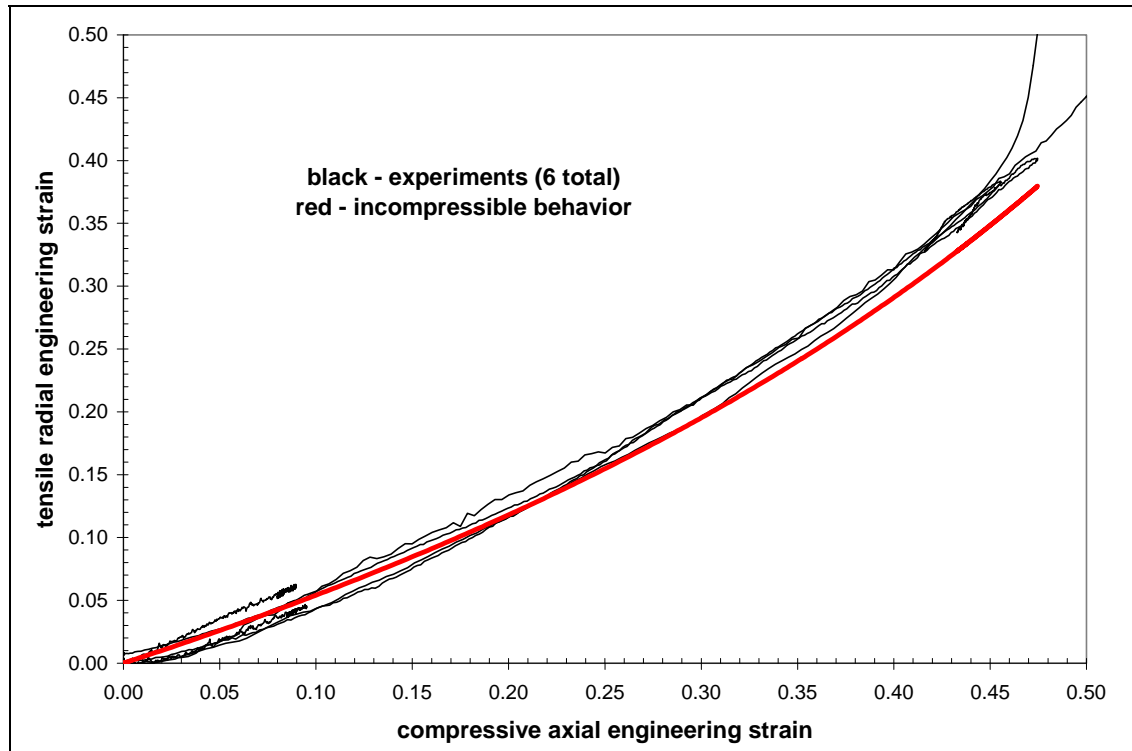


Figure 2. Lateral strain as measured by a laser extensometer in the SHPB tests plotted in figure 1 (thin black curves). The heavy red curve shows that which would be expected from incompressible behavior.

would result from incompressible deformation. The agreement is good, and what deviation can be measured could easily be explained by barreling. Therefore, the remainder of this report will speak in terms of true stress and strain as calculated from the engineering values under the assumption of incompressibility. These terms and the assumption of incompressibility are reviewed in the appendix.

Figures 3 and 4 show the true stress-strain curves for the tests of figure 1. The data are plotted with two scales to show more detail in the low-strain range. Figure 5 shows the rate of true strain for the SHPB experiments. Note that in all cases the strain rate is reasonably constant. The low-rate tests are controlled in the servo-hydraulic load frame to give constant rates of true strain. Figure 6 shows stress at 7% strain as a function of strain rate, and shows the trend of rate-hardening of this material.

Figure 7 shows the stress-strain curves from the experiments at 4000/s, which were conducted at initial temperatures of 22, 43, 56, and 78 °C. A substantial softening is observed over this range of temperatures. Stresses at a strain of 10% are plotted with temperature in figure 8. From this graph, it is apparent that the softening is approximately linear with stress over the range of 22–56 °C. As seen in figure 7, there is a significant change in the form of the stress-strain curve for the 78 °C test. It is suggested that this may be due to a phase change in the PTFE that occurs at some temperature between 56 and 78 °C, although this is merely speculative.

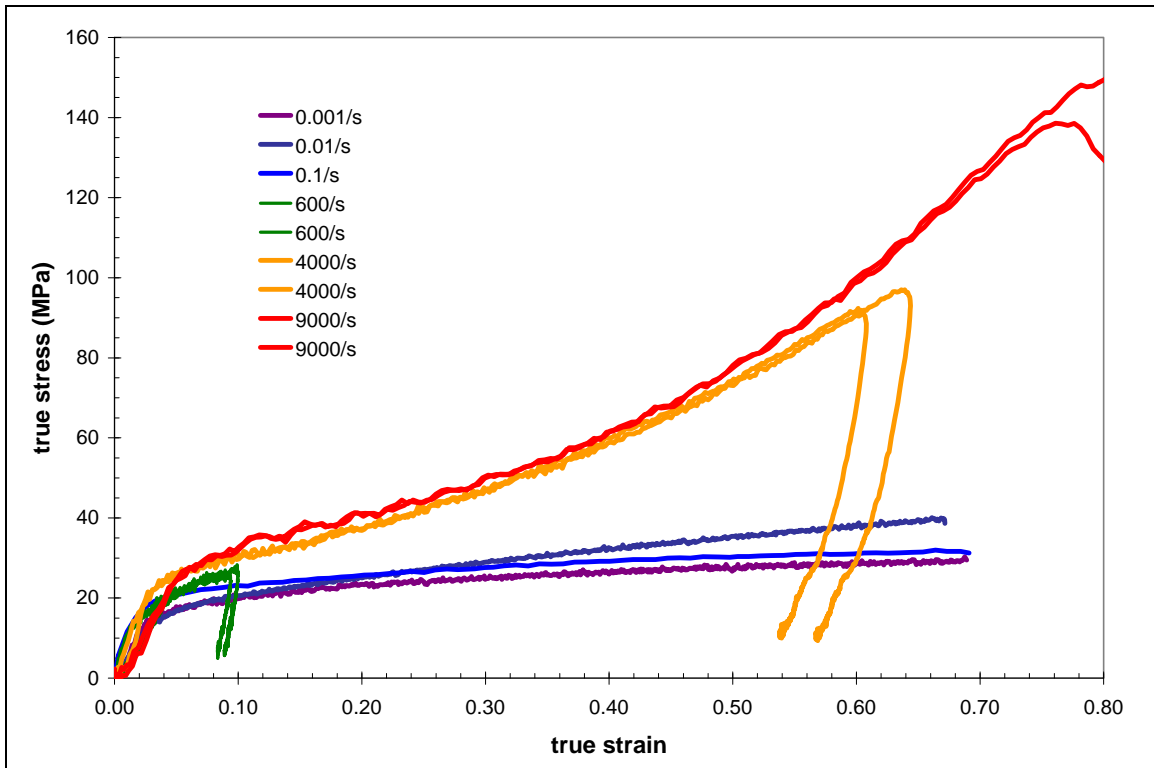


Figure 3. True stress-strain curves for Al/PTFE. All samples were initially at room temperature (22 °C).

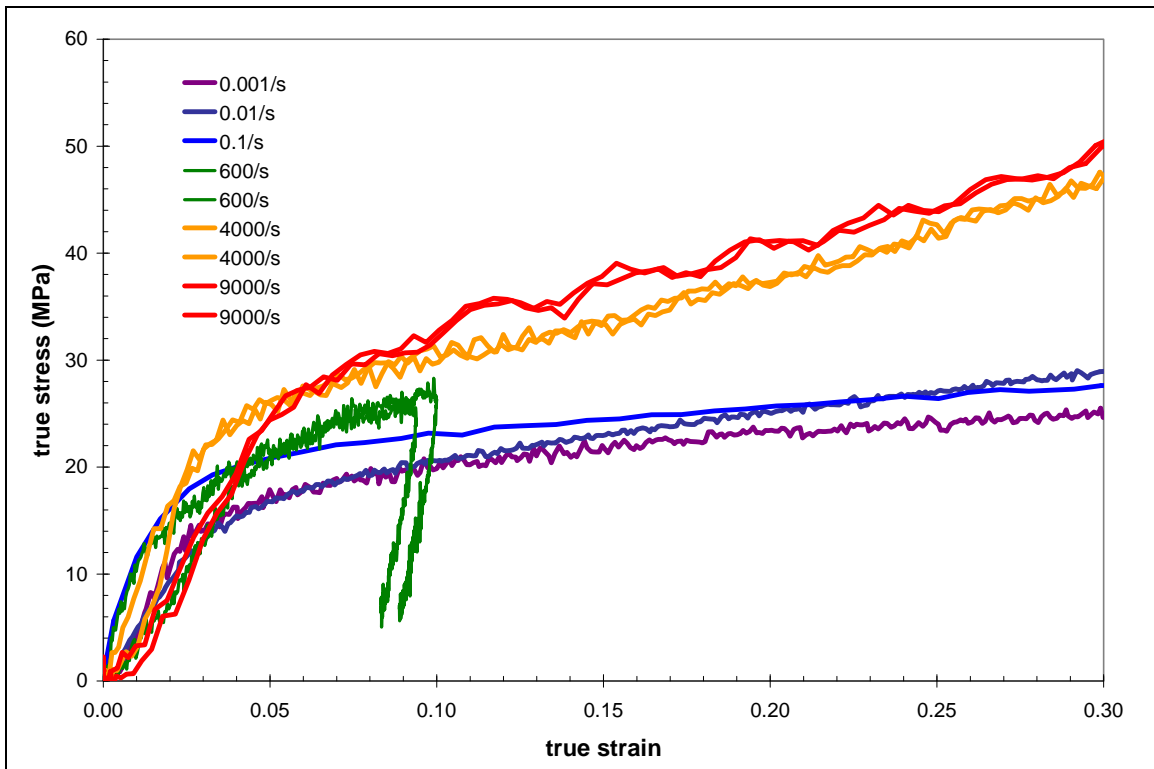


Figure 4. The data of figure 3 repeated on a finer scale to illustrate the low-strain behavior.

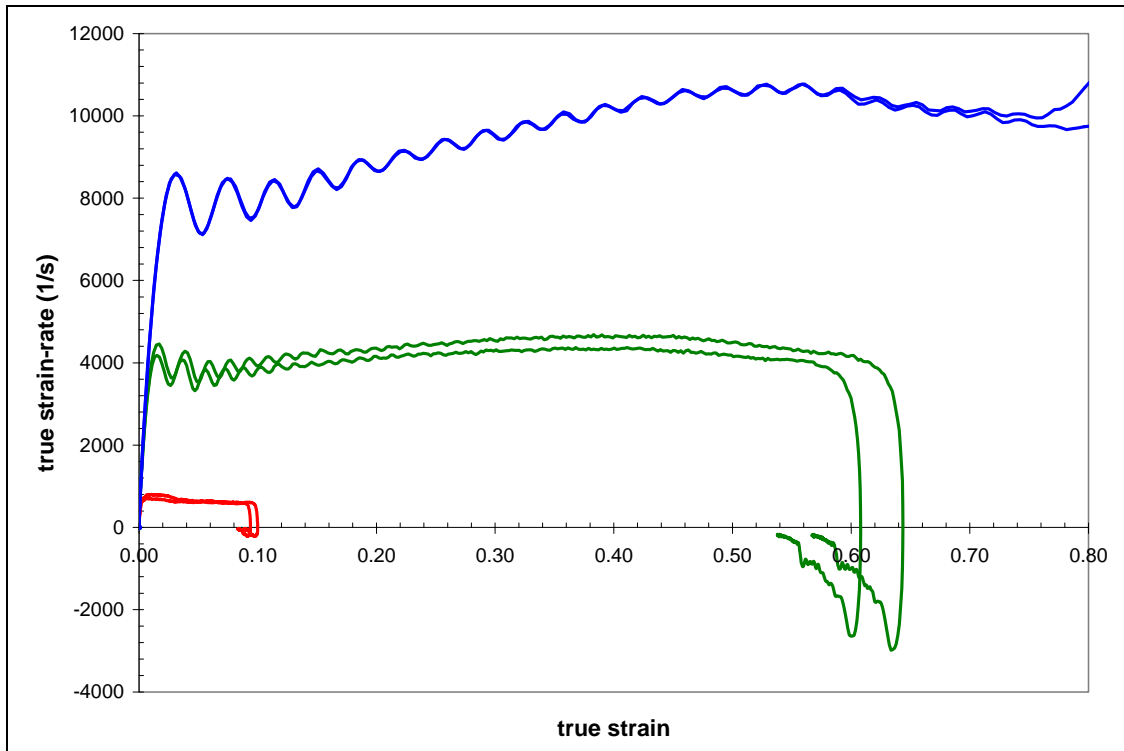


Figure 5. The variation of true strain rate for the SHPB tests.

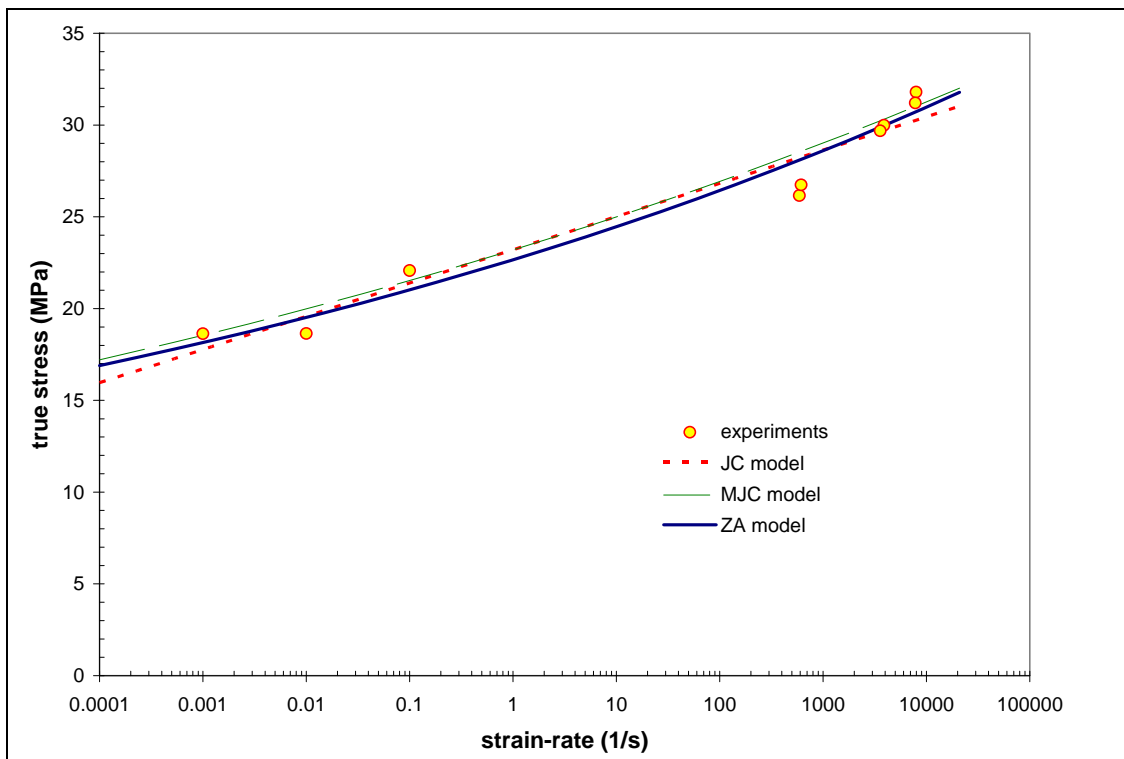


Figure 6. Strain-rate hardening observed in the experiments compared to the MJC, JC, and ZA fits. Stress is measured at 7% total true strain, all at room temperature (295 K).

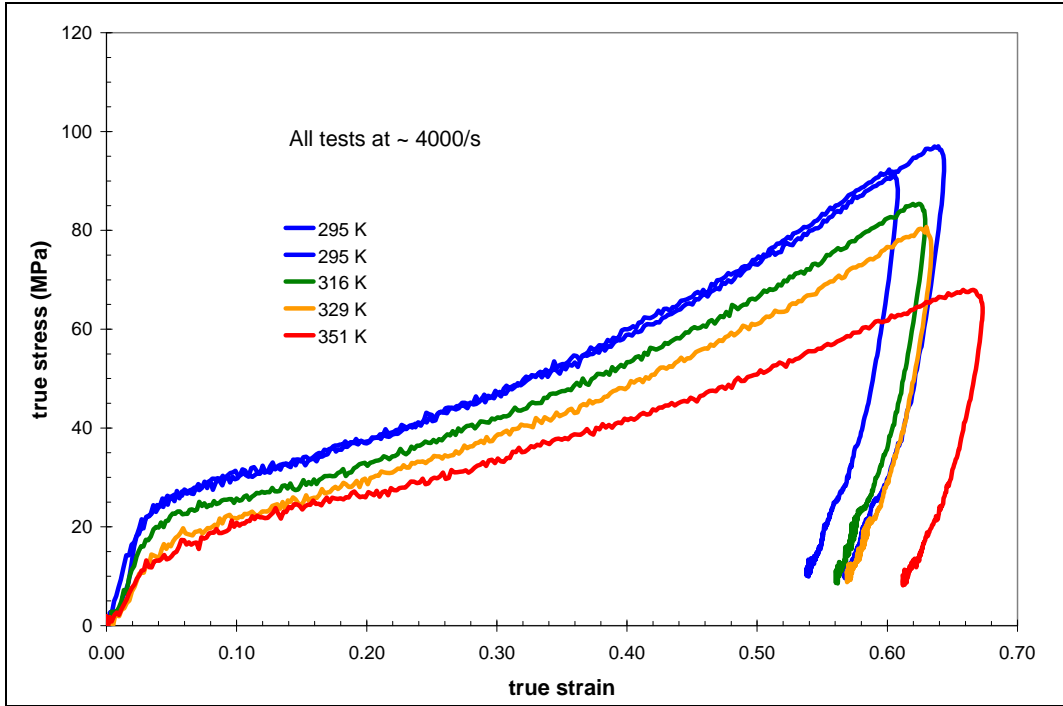


Figure 7. Stress-strain curves obtained at a rate of 4000/s over a range of initial temperatures.

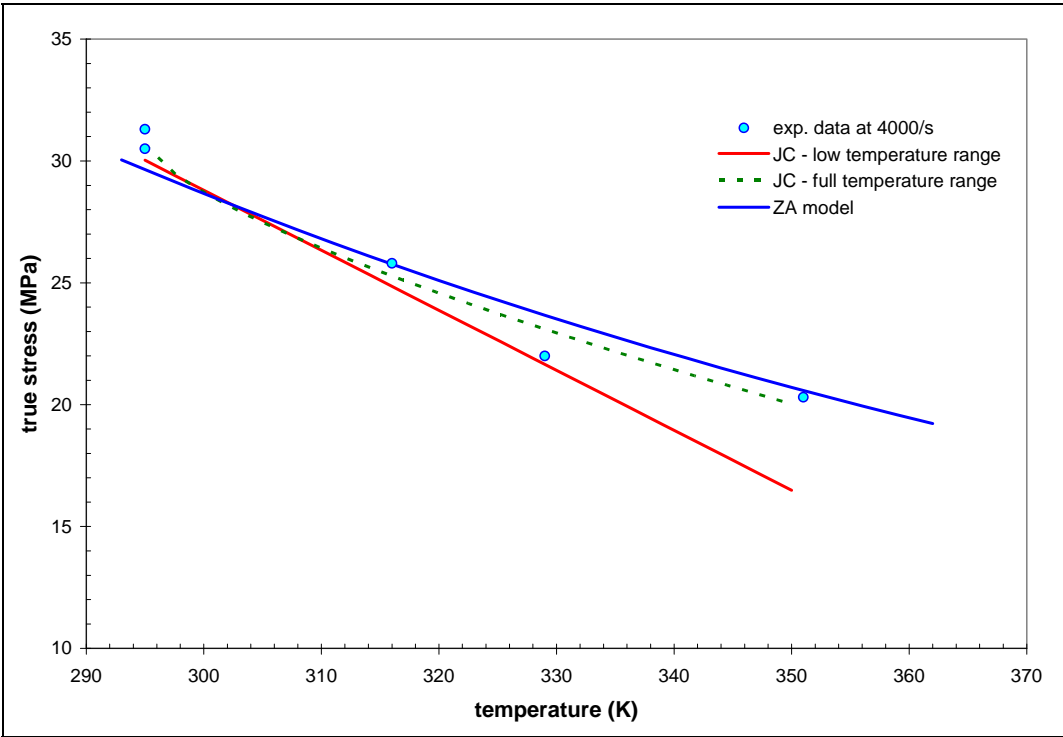


Figure 8. Three fits to the high-rate temperature data (10% total strain, 4000/s). The JC equation is fit over two temperature ranges: the lower temperature range of $295 \text{ K} \leq T \leq 329 \text{ K}$ and the full temperature range. A fit is also shown for the ZA model (full range).

5. Constitutive Modeling

5.1 Johnson-Cook and Modified Johnson Cook

The data of the preceding sections have been fitted to the JC and MJC constitutive equations. These models were chosen primarily because of their widespread use, and not necessarily because they are particularly well-suited to this material. Details of the models are discussed in Johnson and Cook (5) and Holmquist and Johnson (6), and are reviewed briefly in the following.

The JC and MJC equations are written as

$$\sigma = (A + B\varepsilon_p^n) \left(1 + C \ln \left(\frac{\dot{\varepsilon}}{\dot{\varepsilon}_0} \right) \right) (1 - T^{*m}), \quad (1)$$

and

$$\sigma = (A + B\varepsilon_p^n) \left(\frac{\dot{\varepsilon}}{\dot{\varepsilon}_0} \right)^\lambda (1 - T^{*m}), \quad (2)$$

respectively, where T^* is the homologous temperature,

$$T^* = \frac{T - T_r}{T_m - T_r}. \quad (3)$$

The term ε_p denotes plastic strain, i.e., the total strain less the elastic strain, assumed in the following fits to be 3.5%. A , B , n , C , λ , and m are all material constants. T_m , which is generally taken as the melting temperature, is here treated as a free-parameter to improve the quality of the fits. T_r is a reference temperature, 295 K, the temperature of the lowest temperature tests. Note that the form of the thermal softening term is in general not defined for $T < T_r$, so extrapolation below T_r is not possible. The reference strain-rate, $\dot{\varepsilon}_0$, is taken as 1/s.

The only difference in the two equations is the form of the strain-rate hardening; the original version uses a logarithmic form and the modified version uses a power-law form. The form of the equations, $\sigma = f(\varepsilon) \cdot g(\dot{\varepsilon}) \cdot h(T)$, is very convenient for fitting the available data. By assuming $\varepsilon \sim 0$ and $T = 295$ K in equation 1, estimates of A and C can be determined from a simple least squares fit to the rate data of figure 6. This can then be repeated with equation 2, giving estimates for A and λ for the MJC equation.

Next, the temperature data of figure 8 can be fit to each equation under the assumptions that $\varepsilon \sim 0$ and $\dot{\varepsilon} = 4000$ /s to give estimates of A , m , and T_m . Two fits are made, one over the lower three temperatures, a range of $T \in [295, 329]$ K, and the other the full range $T \in [295, 351]$ K. The former provides the better fit, and it is suggested that it be used if temperatures above 329 K are not encountered.

The strain-hardening terms, A, B, and n, can be fit to the stress-strain curves of figure 3, under the assumption that the high-rate curves are adiabatic and the low-rate curves are isothermal. This is done in an ad hoc manner to roughly match the data. To fit the adiabatic curves, it is assumed that c_v , the specific heat capacity, is 1160 J/kg-K, based on an estimate used by Raftenberg et al. (7). The conversion of plastic work to heat, β , is assumed to be 0.9.* Finally, the parameters are arbitrarily adjusted such that the overall fit of the model adequately matches the experimental data of figures 3, 4, 6–8, simultaneously, using the actual conditions at which those graphs present the data (e.g., actual plastic strain values, adiabatic/isothermal conditions). More sophisticated fitting procedures can be developed but are hardly justifiable as they do not offer any real improvement to the quality of the fit obtained.

Four sets of final parameters are given in table 1, for each model over the two temperature ranges mentioned above. Comparisons of selected model fits against the experimental data are given in figures 6, 8, 9, and 10. In general, the difference between the quality of the fits between the JC and MJC is small, with the MJC providing a slightly superior fit to the data (see figure 6) in a least-squares-residuals sense. Because there is no rate dependence of the strain-hardening terms, neither model is able to capture the strain-hardening effect at both high (>600/s, figure 9) and low (<0.1/s, figure 10) rates. This is obvious in the figures. Because it is anticipated that these models will be applied to high-rate scenarios, the data is fit to the high-rate data essentially ignoring the strain hardening observed at the low rates. Users are cautioned against using these parameter sets if their problems involve significant deformation at low rates.

Table 1. JC and MJC constants for Al/PTFE. The fits are performed over two temperature ranges.

Parameter	295 K ≤ T ≤ 329 K		295 K ≤ T ≤ 351 K		Unit of Measurement
	JC	MJC	JC	MJC	
A	22.71	22.71	22.71	22.71	MPa
B	160	160.1	160	160	MPa
n	1.8	1.8	1.8	1.8	—
C	0.0339	Not used	0.0339	Not used	—
λ	Not used	0.0324	Not used	0.0324	—
$(d\epsilon/dt)_0$	1	1	1	1	s^{-1}
m	1	1	0.707	0.707	—
T_m	417	417	541	541	K
T_r	295	295	295	295	K
ρ	2290	2290	2290	2290	kg/m ³
c_v	1161	1161	1161	1161	J/kg-K

Note: T_m as used here is simply a free-parameter in the fitting process and is not the melting temperature of the material.

*Rae and Dattelbaum (8) measured the beta factor for pure PTFE and found it to be in the range from 0.8 to 0.6 at room temperature and at a strain rate of 10/s.

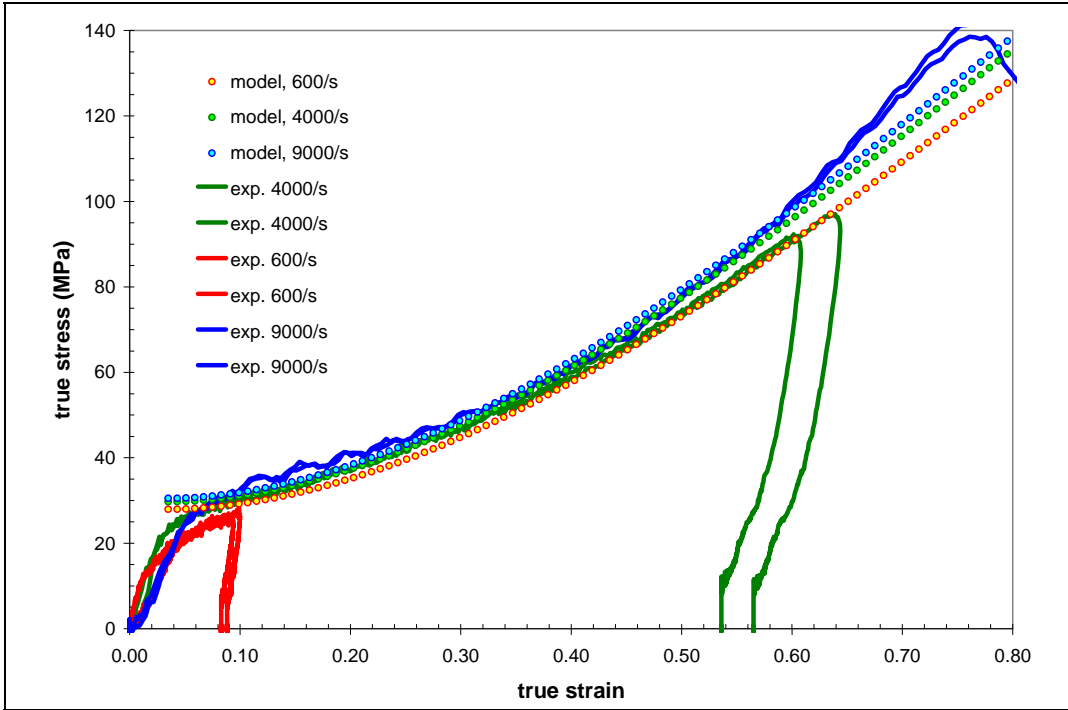


Figure 9. MJC model predictions, assuming adiabatic conditions, compared to the high-rate (SHPB) data. The JC model predictions are essentially identical.

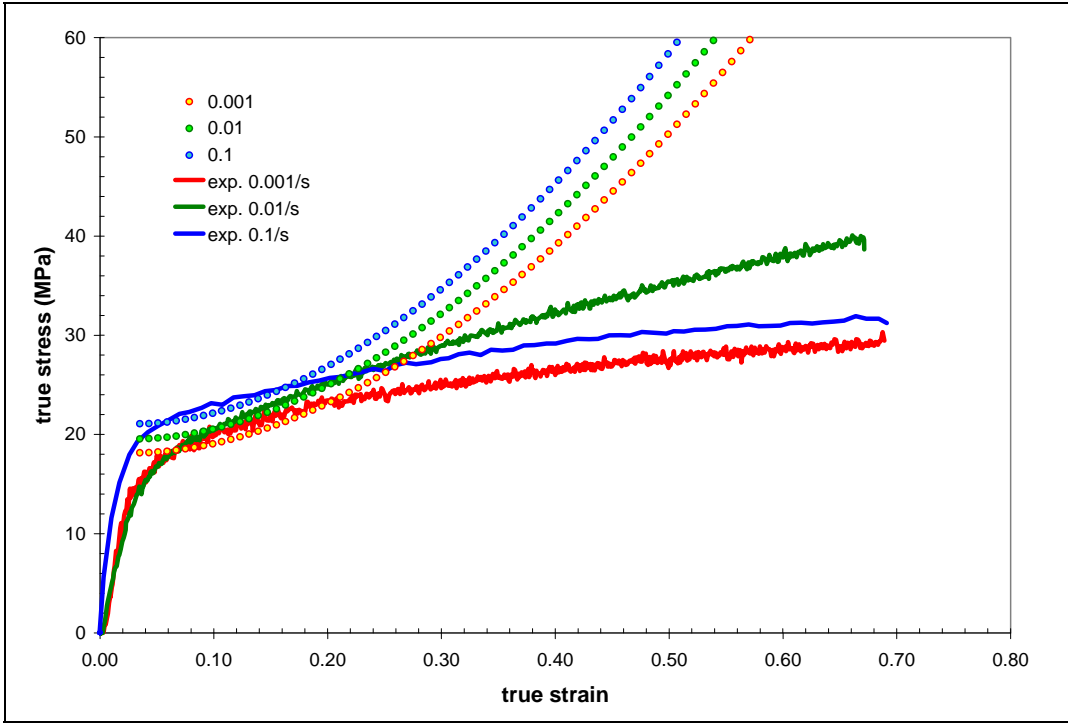


Figure 10. MJC model predictions, assuming isothermal deformations, compared to the low-rate experiments. The JC model predictions are essentially identical.

5.2 Zerilli-Armstrong Model for Polymers

Zerilli and Armstrong have developed constitutive models for metals based on thermally activated dislocation motion (9, 10). Recently, they have adapted the basic framework to apply to viscoplastic deformation of polymers (11, 12). They have used it to model PTFE (11), and Cai et al. (13) have used it to model a composite mixture of PTFE-Al-W. Based on the success of these applications, it was decided to use this model to represent the present data. Although the model is physically based, the approach taken here is to treat it as a curve fit, i.e., the values presented below may not necessarily be realistic beyond the observation that they match the existing data.

The Zerilli-Armstrong equation for polymers relates effective stress, σ , to effective plastic strain, ϵ_p , temperature, T , and pressure, p , according to

$$\sigma = B e^{-\beta T} + B_0 \sqrt{\frac{1 - e^{-\omega \epsilon_p}}{\omega}} e^{-\alpha T}, \quad (4)$$

where

$$\beta = \beta_0 - \beta_1 \ln \dot{\epsilon}_p, \quad (5)$$

$$\alpha = \alpha_0 - \alpha_1 \ln \dot{\epsilon}_p, \quad (6)$$

$$\omega = \omega_a + \omega_b \ln \dot{\epsilon}_p + \omega_p p, \quad (7)$$

$$B = B_{pa} (1 + B_{pb} p)^{B_{pn}}, \quad (8)$$

and

$$B_0 = B_{0pa} (1 + B_{0pb} p)^{B_{0pn}}. \quad (9)$$

There are 13 parameters that need to be determined. Due to the relatively limited set of data and the complexity of the model, a number of parameters are set to be zero. Foremost, all parameters leading to a pressure dependent yield stress are set to zero. This is not to imply that the material has no pressure dependence, the data is simply not available.* Thus, $B_{pb} = \omega_p = B_{0pn} = B_{pn} = B_{0pb} = 0$, and the model simplifies to

$$\sigma = B_{pa} e^{-(\beta_0 - \beta_1 \ln \dot{\epsilon}_p)T} + B_{0pa} \sqrt{\frac{1 - e^{-(\omega_a + \omega_b \ln \dot{\epsilon}_p)\epsilon_p}}{(\omega_a + \omega_b \ln \dot{\epsilon}_p)}} e^{-(\alpha_0 - \alpha_1 \ln \dot{\epsilon}_p)T}. \quad (10)$$

Assuming $\epsilon_p = 0$ and $T = 295$ K, the right-hand term vanishes and a power-law least-squares fit to the rate data (figure 6) can be made.

$$\sigma = (B_{pa} e^{-\beta_0 T}) \dot{\epsilon}_p^{\beta_1 T} \Rightarrow \sigma = k \dot{\epsilon}_p^{\beta_1 T}. \quad (11)$$

* PTFE has been shown to have a pressure dependent flow stress (10).

The constant k and β_1 are determined by the curve fit. Through k , a relationship is established between β_0 and B_{pa} .

$$\beta_0 = -\frac{1}{T} \ln \left(\frac{k}{B_{pa}} \right). \quad (12)$$

Using this relationship and assuming $\dot{\epsilon} = 4000/\text{s}$ and $\epsilon_p = 0$, B_{pa} can be determined by that value which gives an optimum fit to the temperature data of figure 8. Equation 12 then gives β_0 , and the first term on the right-hand side of equation 10 is determined.

The remaining term deals with strain hardening. Aside from the behavior seen in figure 7 at 351 K, which may be due to a phase change, there is no convincing data that the strain hardening changes with temperature, so set $\alpha_0 = \alpha_1 = 0$.^{*} This leaves three terms to be determined: ω_a , ω_b , and B_{0pa} . A least absolute value best fit[†] is made to the stress-strain data shown in figure 3, assuming the high-rate curves are isothermal, i.e., the data are fit to

$$\sigma = B_{pa} e^{-(\beta_0 - \beta_1 \ln \dot{\epsilon}_p)T} + B_{0pa} \sqrt{\frac{1 - e^{-(\omega_a + \omega_b \ln \dot{\epsilon}_p)\epsilon_p}}{(\omega_a + \omega_b \ln \dot{\epsilon}_p)}}, \quad (13)$$

to obtain estimates for ω_a , ω_b , and B_{0pa} . This is technically incorrect, but fortunately the differences between adiabatic and isothermal behaviors for these experiments are not drastically different, and thus the fitting process is simplified.

As with the Johnson-Cook fits, the resulting parameter set is adjusted in an ad hoc manner to obtain the “best” simultaneous fits to the isothermal and adiabatic stress-strain curves, the rate hardening, and the thermal softening. The resulting optimum parameters are listed in table 2, and the quality of the fit is shown against the experimental data in figures 6, 8, 11, and 12. To facilitate comparisons, the parameter sets of Cai et al. (13) for PTFE-Al-W, and Zerilli and Armstrong (11) for PTFE and also listed in the table.

6. Conclusion

The experiments conducted in this program have been used to populate the JC, MJC, and ZA for polymers constitutive models. These models address the inert behavior of the material only. It is worth noting that in none of these experiments was any evidence of a reaction, either during the experiment or post-mortem, observed.

^{*} It was hoped that adjustment of α_0 and α_1 would help produce a better match between the model and the temperature tests at larger deformations. However, this did not appear to be the case so these two parameters were left at zero values.

[†] A numerical technique is used.

Table 2. The ZA constants for Al/PTFE. The values determined by Cai et al. (13) and Zerilli and Armstrong (11) for PTFE-Al-W and PTFE are included for comparison.

Parameter	RM-4	PTFE-Al-W	ZA PTFE	Unit of Measurement
β_0	0.011672	0.020100	0.020100	1/K
β_1	0.000139	0.000264	0.000264	1/K
α_0	0.000000	0.004780	0.004780	1/K
α_1	0.000000	0.000050	0.000050	1/K
ω_a	-3.000	-2000	-3.600	—
ω_b	-0.500	-0.625	-0.625	—
ω_p	0.000	-0.031	-0.040	1/MPa
B_{pa}	550	4016	4016	MPa
B_{pb}	0.000	0.020	0.020	1/MPa
B_{pn}	0.000	0.714	0.714	—
B_{0pa}	25.0	72.4	72.4	MPa
B_{0pb}	0.000	0.022	0.022	1/MPa
B_{0pn}	0.000	0.500	0.500	—

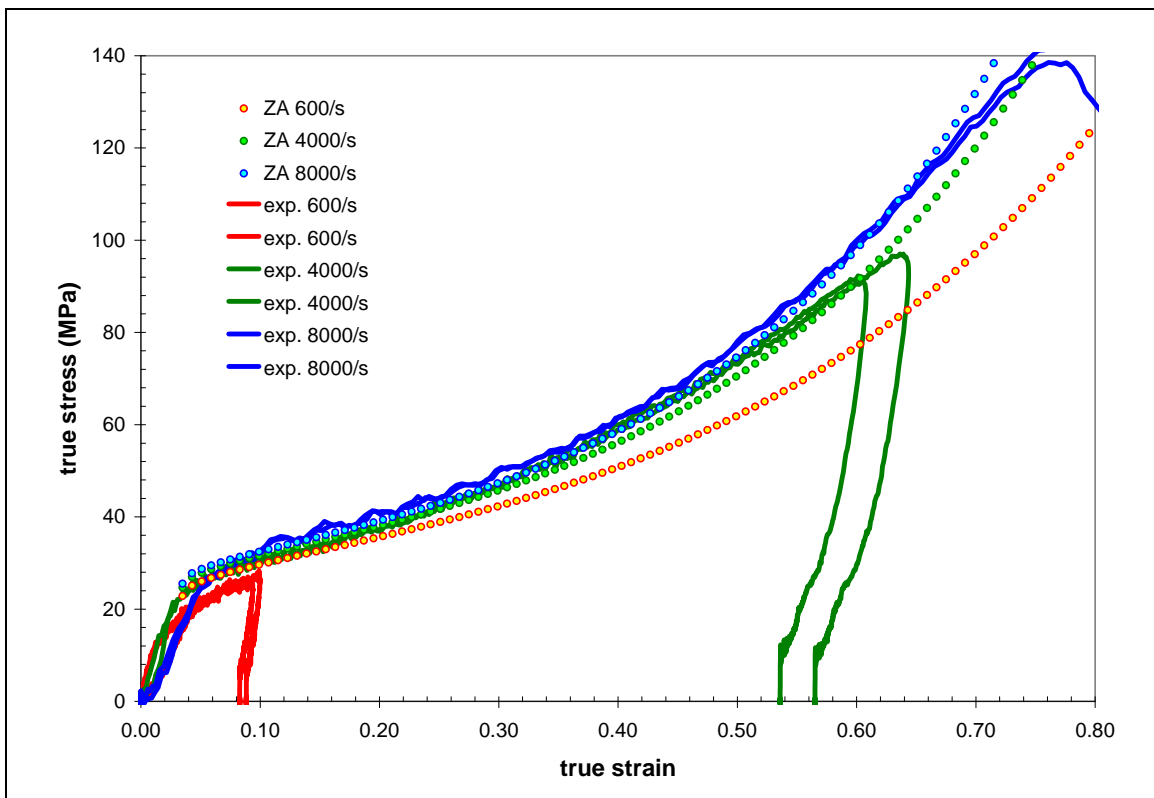


Figure 11. Comparison of the ZA model to the SHPB experiments assuming adiabatic conditions.

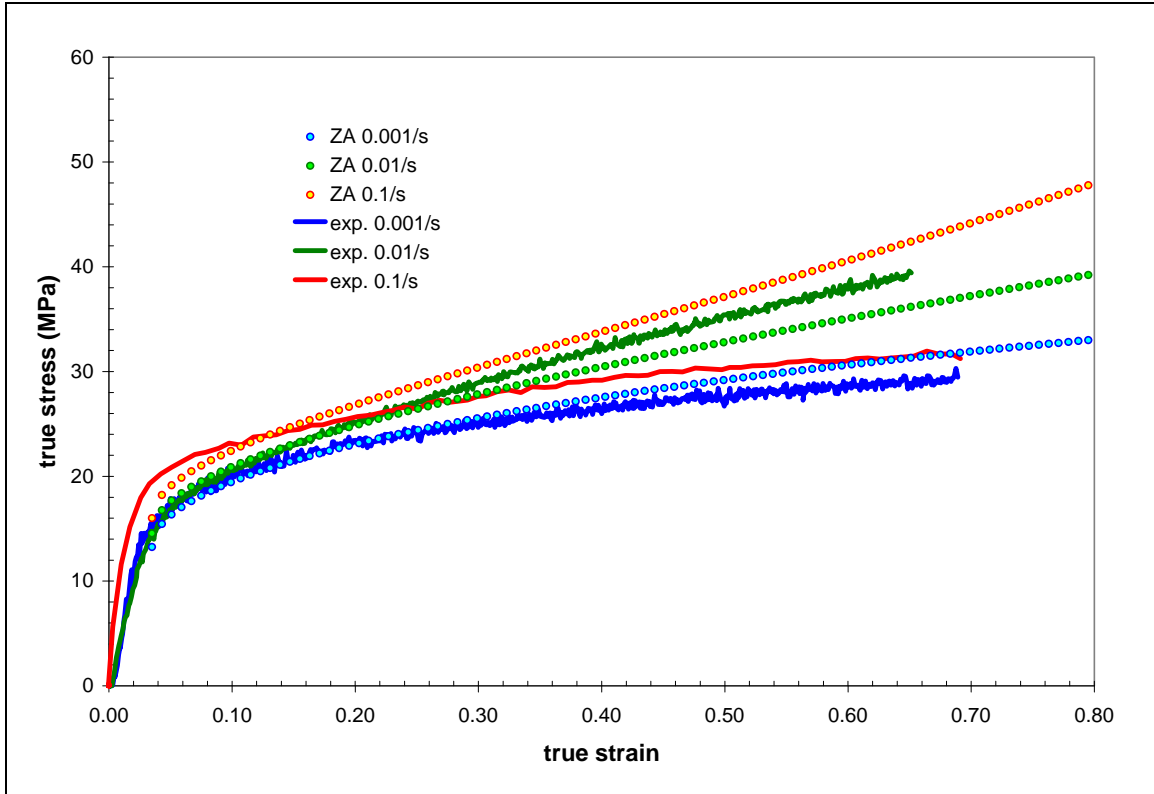


Figure 12. Comparison of the ZA model to the low-rate experiments assuming isothermal conditions. Note the great improvement over the JC fits to the same data, figure 10.

It is believed that these models are suitable for simulations of low-speed impacts (e.g., the cylinder impacts of Casem and Raftenberg [14] and Mock and Holt [15]). However, readers shown remain aware of the comments and caveats made above, especially the inability of the JC models to capture the strain hardening effects over the full range of strain-rates investigated. It is suggested that the JC model could be made to capture this effect by making the strain hardening parameters suitable functions of strain-rate. However, it is recommended that the ZA model, which is more firmly rooted by a physical foundation, be used in place of the JC fits whenever possible. As with any model, readers should exercise caution when using these models outside of their calibrated ranges. Note that the elastic behavior of the material has not been characterized. Any reader who implements this model will need to address this. One should also take care when using these models to represent Al-PTFE mixtures that are not manufactured using this same process. For example, there is a considerable difference between this material behavior and that measured in Raftenberg (7), although superficially both are basically the same mixture.

Finally, failure is not addressed in this work. When failure was observed in these tests, it appeared to be primarily due to ductile fracture. It is not believed that this material exhibits shear banding, and the mechanical properties listed in this work support this (in terms of the relative effects of strain and strain-rate hardening and thermal softening). Some fracture work has been preformed on Al/PTFE composites; refer to Joyce and Joyce (16).

7. References

1. Follansbee, P. S.; Franz, C. Wave Propagation in the Split-Hopkinson Pressure Bar. *J. Eng. Mat. Tech.* **1983**, *105*, 61.
2. Gong, J. C.; Malvern, L. E.; Jenkins, D. A. Dispersion Investigation in the Split-Hopkinson Pressure Bar. *J. Eng. Mat. Tech.* **1990**, *112*, 309–314.
3. Follansbee, P. S. *Metals Handbook*, 8; American Society for Metals: Metals Park, OH, 1985; p 198.
4. Ramesh, K. T.; Narasimhan, S. Finite Deformations and the Dynamic Measurement of Radial Strains in Compression Kolsky Bar Experiments. *Int. J. Solids Struct.* **1996**, *33* (25), 3723–38.
5. Johnson, G. R.; Cook, W. H. A Constitutive Model and Data for Metals Subjected to Large Strains, High Strain Rates, and High Temperatures. *In: Proceedings from the 7th International Symposium on Ballistics*, 1983, pp 541–547.
6. Holmquist, T. J.; Johnson, G. R. Determination of Constants and Comparison of Results for Various Constitutive Models. *J. de Physique IV* **1991**.
7. Raftenberg, M.; Mock, W.; Kirby, G. Modeling the Impact Deformation of Rods of a Pressed PTFE/Al Composite Mixture. Accepted for publication in *Int. J. Impact Eng.*
8. Rae, P. J.; Dattelbaum, D. M. The Properties of poly(tetrafluoroethylene) (PTFE) in Compression. *Polymer* **2004**, *45*, 7615–7625.
9. Zerilli, F. J.; Armstrong, R. W. Dislocation-Mechanics Based Constitutive Relations for Material Dynamics Calculations. *J. Appl. Phys.* **1987**, *61* (5), 1816–1825.
10. Zerilli, F.; Armstrong, R. J. Description of Tantalum Deformation Behavior by Dislocation Mechanics Based Constitutive Relations. *Appl. Phys.* **1990**, *68*, 1580–1591.
11. Zerilli, F.; Armstrong, R. A Constitutive Equation for the Dynamic Deformation Behavior of Polymers. *J. Material Sci.* **2007**, *42* (12), 4562–4574.
12. Zerilli, F.; Armstrong, R. Thermal Activation Based Constitutive Equations for Polymers. *J. Phys. IV France* **2000**, *10*, Pr9.3–8.
13. Cai, J.; Walley, S.; Hunt, R.; Pround, W.; Nesterenko, V.; Meyers, M. High-Strain, High Strain-Rate Flow and Failure in PTFE/Al/W Granular Composites. *Mater. Sci. Eng. A* **2007**, doi:10.1016/j.msea.2007.03.068.

14. Casem, D.; Raftenberg, M. Initiation Experiments on Aluminum/PTFE. *Proceedings of the 2006 JANNAF Conference*, San Diego, CA, December 2006.
15. Mock, W.; Holt, W. Impact Initiation of Rods of Pressed Polytetrafluoroethylene (PTFE) and Aluminum Powders. In: *Shock Compression of Condensed Matter-2005*, 2006; 1097.
16. Joyce, J.; Joyce, P. Toughness Characterization of a Metal Filled PolyTetraFlouroEthylene using the J-integral. *Eng. Fracture. Mech.* **2004**, *71*, 2512–2531.

Appendix. Strain Measures Defined

This appendix clarifies the definitions of engineering stress and strain and true stress and strain as used in this report. The unqualified use of any of these terms implies positive values in compression.

Engineering stress, s , is defined as

$$s = \frac{P}{A_0}, \quad (\text{A-1})$$

where P is the compressive load applied to the specimen and A_0 is its original cross-sectional area.

True stress, σ , is defined as

$$\sigma = \frac{P}{A}, \quad (\text{A-2})$$

where A is the instantaneous cross-sectional area of the specimen, i.e., the area at any instant in time as the specimen deforms.

Engineering strain, e , is defined by

$$e = \frac{\delta}{L_0}, \quad (\text{A-3})$$

where δ is the amount the specimen is compressed and L_0 is the initial length of the specimen. Note that L , the instantaneous length, can then be found by $L = L_0 - \delta$.

True strain, ε , is defined by

$$d\varepsilon = -\frac{dL}{L}. \quad (\text{A-4})$$

Here, dL is an increment in specimen length, i.e., the negative sign is needed to make this positive in compression. This can be integrated for the conditions of the compression test to give

$$\varepsilon = -\ln\left(\frac{L}{L_0}\right). \quad (\text{A-5})$$

By equation (A-3), true strain can be related to engineering strain by

$$\varepsilon = -\ln(1 - e). \quad (\text{A-6})$$

If the deformation of a specimen is incompressible, and if the initially cylindrical specimen remains cylindrical during the deformation process,* the instantaneous volume is equal to the initial volume at any instant, i.e.,

$$d^2L = d_0^2L_0, \quad (\text{A-7})$$

where d_0 and d are the initial and instantaneous diameters of the specimen. Using this relationship, true stress can be determined from the engineering quantities by

$$\sigma = s(1 - e). \quad (\text{A-8})$$

Furthermore, the *tensile* radial engineering strain of the specimen, defined as

$$e_r = \frac{d - d_0}{d_0}, \quad (\text{A-9})$$

can be related to the axial engineering strain of the specimen by

$$e_r = \frac{1}{\sqrt{1 - e}} - 1. \quad (\text{A-10})$$

This applies only to incompressible behavior. It is this equation that was plotted in figure 2 of this report.

*This is only approximately true in compression testing because of “barreling” that occurs due to friction at the platens.

NO. OF
COPIES ORGANIZATION

1 DEFENSE TECHNICAL
(PDF INFORMATION CTR
ONLY) DTIC OCA
8725 JOHN J KINGMAN RD
STE 0944
FORT BELVOIR VA 22060-6218

1 US ARMY RSRCH DEV &
ENGRG CMD
SYSTEMS OF SYSTEMS
INTEGRATION
AMSRD SS T
6000 6TH ST STE 100
FORT BELVOIR VA 22060-5608

1 DIRECTOR
US ARMY RESEARCH LAB
IMNE ALC IMS
2800 POWDER MILL RD
ADELPHI MD 20783-1197

1 DIRECTOR
US ARMY RESEARCH LAB
AMSRD ARL CI OK TL
2800 POWDER MILL RD
ADELPHI MD 20783-1197

1 DIRECTOR
US ARMY RESEARCH LAB
AMSRD ARL CI OK T
2800 POWDER MILL RD
ADELPHI MD 20783-1197

ABERDEEN PROVING GROUND

1 DIR USARL
AMSRD ARL CI OK TP (BLDG 4600)

NO. OF
COPIES ORGANIZATION

ABERDEEN PROVING GROUND

10 DIR USARL
AMSRD ARL WM TD
D CASEM